An Acad Bras Cienc (2021) 93(1): e20200236 DOI 10.1590/0001-3765202120200236
Anais da Academia Brasileira de Ciências | *Annals of the Brazilian Academy of Sciences*
Printed ISSN 0001-3765 I Online ISSN 1678-2690
www.scielo.br/aabc | www.fb.com/aabcjournal

GEOSCIENCES

Geochemical and reflectance spectroscopy data integration to characterize emerald deposits: the case of the Paraná deposit, Brazil

JOSÉ F. ARAÚJO NETO, SANDRA B. BARRETO, THAIS A. CARRINO, IGOR M.B.A. SOUZA & GLENDA L. SANTOS

Abstract: The Paraná emerald deposit is one of the few occurrences of emerald, a rare beryl variety, in Borborema Province, northeastern Brazil. We characterized the Paraná deposit by combining field geology, petrography, whole-rock geochemistry, mineral chemistry, and reflectance spectroscopy. The mineralization is associated with phlogopite-, actinolite-phlogopite-, and phlogopite-phengite schists, mylonitic gneisses, and several acidic rocks (*e.g.* granitic pegmatites/aplites, quartz ± feldspar veins) along the Portalegre Shear Zone. Emerald can be found in quartz-feldspar and aplite veins and veinlets interleaved with phlogopite- or actinolite-phlogopite schists, or within the foliation of the schists. The presence of albitites and the compositional variation of the schists suggest a metasomatic origin for emerald with variations of the metasomatic process. All these different lithotypes can be readily identified through reflectance spectroscopy especially in the range of 2,150-2,450 nm, where the main mafic minerals show absorption features related to Al-OH (phengite), and Fe-OH and Mg-OH bonds (phlogopite/actinolite). Our study shows that possible mineralized phlogopite schists can be distinguished from other sterile rocks, although point spectral analysis does not separate emerald-bearing phlogopite schists from schists without emerald due to the dominance of major phlogopite absorption features rather than emerald features.

Key words: Geochemistry, mineral chemistry, Paraná emerald deposit, petrography, reflectance spectroscopy.

INTRODUCTION

Knowledge about gem-quality mineral deposits within the Borborema Province, northeastern Brazil, was concentrated for years in the Seridó Pegmatite Province (SPP, previously known as the Borborema Pegmatite Province; Scorza 1944), since the First World War, due to its large amount of industrial minerals (especially mica), until the end of the Second World War, as a result of the search for strategic materials such as tantalum and beryllium minerals (Silva et al. 1995, Beurlen et al. 2009, Santos et al. 2014).

Over the last two decades, a few other Brazilian gemological districts have been recognized outside the SPP, such as the Solonópole-Quixeramobim Pegmatite District (Ceará state; Vidal & Nogueira Neto 2005), the Cristais-Russas Pegmatite District (Ceará state; Vidal & Nogueira Neto 2005), and the Extreme Southwest Gemological District (Rio Grande do Norte state; Moraes 1999). The latter is known for amazonite and dark blue aquamarine mineralizations associated with granitic pegmatites in the Vieirópolis Pegmatite Field (Barreto et al. 2016), as well as emerald-bearing schists within the so-called Paraná – Marcelino

Vieira – Francisco Dantas emerald belt (Moraes 1999).

This emerald belt stands out as one of the few occurrences of this rare dark green variety of beryl in Borborema Province (*cf.* Schwarz 1987, Giuliani et al. 1990, Zwaan et al. 2012, Santiago et al. 2018). The best emerald crystals have been recovered from the vicinity of Paraná city, specifically from the localities of Pitombeiras and Aroeira, which comprise the Paraná emerald deposit.

Several technical reports have described emeralds from the Pitombeiras and Aroeira mines since the 1980s (*e.g.* Vasconcelos 1984, Moraes 1999, Medeiros 2008, Souza 2017). Araújo Neto et al. (2019) characterized the mineralogy and gemology of the emerald crystals, but detailed studies on the geology remain unveiled.

In this paper, we present a comprehensive geological description of the Paraná deposit by combining field geology, petrography, whole-rock geochemistry, mineral chemistry and reflectance spectroscopy data to understand the relations between the main lithotypes and emerald mineralization.

Reflectance spectroscopy is a non-destructive method that studies the interaction of electromagnetic radiation with a material's surface in the visible to the short-wave infrared spectral range. For rocks and minerals, this interaction can unveil variations on the chemical composition and crystalline structure of each investigated sample. In the visible-near infrared range (VNIR: 400-1,000 nm), electronic transition processes commonly occur in transition metals (*e.g.* Fe, Cr, Ni, Co; Clark 1999, Thompson et al. 1999, Silva et al. 2009), generating diagnostic absorption features. Also, molecular vibrational processes (*e.g.* H-O-H, Al-OH, Fe-OH, C-O) cause absorption features in the short-wave infrared range (SWIR: 1,000-2,500 nm) (Clark 1999, Thompson et al. 1999). In general, the use of reflectance spectroscopy has been well-stated as an exploration method for metal deposits related to hydrothermal alteration systems (Bedell et al. 2009, Kerr et al. 2011, Swayze et al. 2014, Ramakrishnan & Bharti 2015, Carrino et al. 2018). However, its applications are still very uncommon in gemstone deposits (*cf.* Turner et al. 2017).

Emerald mineralization is commonly related to mafic/ultramafic rocks containing ferroan-magnesian mica and amphibole. The emerald absorption features associated with electronic transitions in Cr^{3+} and/or V^{3+} are responsible for its green coloration (Wood & Nassau 1968). On the other hand, ferroan-magnesian mica and amphibole species can be identified by spectral responses in specific wavelength intervals in the VNIR-SWIR range due to their contents of Fe, Mg, Al and OH^- (Pontual et al. 2008).

In this context, we introduce the use of reflectance spectroscopy data as a tool for the characterization of emerald host and associated rocks in a case study in NE Brazil.

Regional geological setting

The Borborema Province, located in northeastern Brazil, is a complex mosaic-like region folded during the Brasiliano Cycle (Almeida et al. 1981). This province covers an area of approximately 400,000 km², and it consists of local exposures of Archean nuclei and large outcrops of Paleoproterozoic gneiss-migmatite basement rocks covered and/or interleaved with Meso- to Neoproterozoic domains marked by supracrustal sequences. All these rock units were intensely affected by regional metamorphism and magmatism of the Brasiliano-Pan African orogeny (800-500 Ma, Brito Neves et al. 2014).

Many authors have conventionally subdivided this province into several domains or sub-provinces based on its structural configuration allied with geochronological and

geophysical data (*e.g.* Brito Neves et al. 2000, Van Schmus et al. 2008, Santos et al. 2010, 2014). According to Santos et al. (2014), the following subdivisions are recognized: (1) three sub-provinces to the north of the Patos Lineament (also known, together, as the Northern Sub-province), named as the Médio Coreaú (MCS), Ceará Central (CCS), and Rio Grande do Norte (RNS) sub-provinces; (2) the Transversal Sub-province (TRS), situated between the Patos and Pernambuco lineaments; and (3) the Meridional Sub-province (MES) that lies on the south of the Pernambuco Lineament (Figure 1a).

The Rio Grande do Norte Sub-province is a Rhyacian to Orosirian crustal block bordered to the south by the Patos Lineament and to the west by the Senador Pompeu Shear Zone (Brito Neves et al. 2000). According to Brito Neves et al. (2000) and Angelim (2006), three main domains compose the RNS: the São José do Campestre (SJD), the Rio Piranhas-Seridó (RPD), and the Jaguaribeano (JGD) domains. The studied area is situated between the Jaguaribeano (west) and Rio Piranhas-Seridó (east) domains, which are limited by the Portalegre Shear Zone (Figure 1b, Brito Neves et al. 2000), a crustal discontinuity

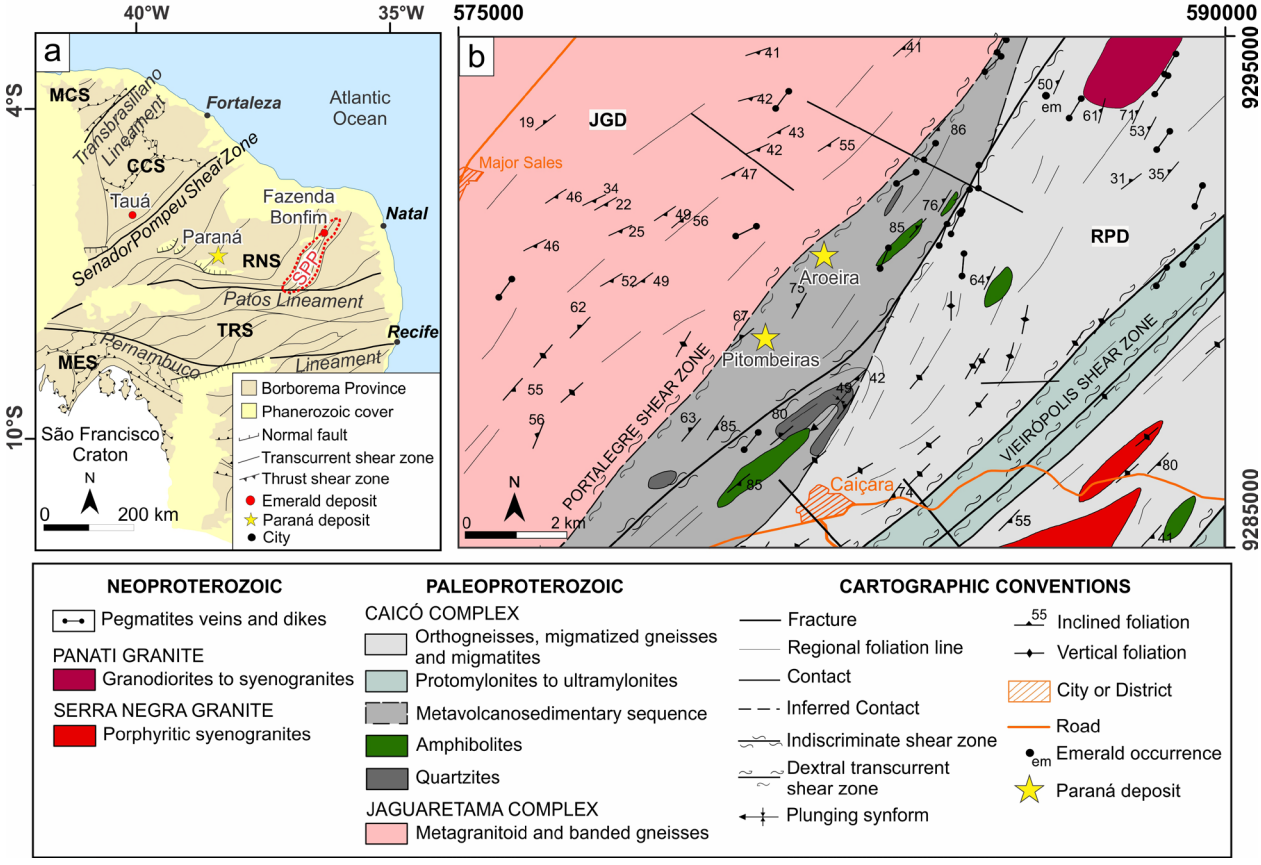

Figure 1. Geological setting of the Paraná deposit. (a) Tectonic subdivision of Borborema Province with the main emerald deposits (Tauá, Paraná and Fazenda Bonfim). Modified from Santos et al. (2014). (b) Local geological map of the Paraná region showing the main emerald mines: Pitombeiras and Aroeira. Modified from Araújo Neto et al. (2018). MCS: Médio Coreaú Sub-province; CCS: Ceará Central Sub-province; RNS: Rio Grande do Norte Sub-province; TRS: Transversal Sub-province; MES: Meridional Sub-province; SPP: Seridó Pegmatite Province; JGD: Jaguaribeano Domain; RPD: Rio Piranhas-Seridó Domain.

that extends from the Patos Lineament to south to the Potiguar Basin to the north.

The Paraná emerald mineralization occurs within the Portalegre Shear Zone (Figure 1b), in a discontinuous trend with, at least 20 km length. The emerald crystals are found mostly inside quartz-feldspar and aplite veins and veinlets interleaved with phlogopite schists. These schists occur as lenticular bodies along the mylonitic fabric of the metavolcanosedimentary unit of the Caicó Complex, which also comprises spatially associated gneisses, amphibolites and quartzites (Moraes 1999, Araújo Neto et al. 2018, 2019).

MATERIALS AND METHODS

Lithological and structural data were collected from several outcrops in the Paraná emerald deposit, mainly from the Pitombeiras and Aroeira mines. The relation between schist and host rocks could be better studied in the Pitombeiras region due to a high number of shafts and trenches.

An Olympus BX51 microscope coupled with an Olympus DP26 camera system was employed for petrographic studies of 67 thin sections.

Forwhole-rockgeochemicalcharacterization, four schist samples were crushed and powdered in the laboratory facilities of the Stable Isotope Laboratory of the Nucleus of Geochemical Studies (NEG-LABISE) at the UFPE. These powders were sent to the Bureau Veritas Mineral Laboratories in Vancouver (Canada) for bulk chemical analyses. After lithium borate fusion, major element concentrations were obtained by inductively coupled plasma emission spectrometry (ICP-ES), while minor and trace elements were determined by inductively coupled plasma mass spectrometry (ICP-MS).
Mineral compositions were determined for nine samples by electron probe micro-analysis (EPMA) using a JEOL JXA-8230 instrument in the Electron Microprobe Laboratory (LASON) of the University of Brasília (UnB). The microprobe is equipped with a scanning electron microscope (SEM), an optical microscope, and a CCD video camera for imagery, five wavelength dispersive X-ray spectrometers (WDS) for quantitative chemical analysis, and one energy dispersive X-ray spectrometer (EDS) for qualitative and/or semi-quantitative analysis. The system was operated for standard silicate analysis, using LASON's internal standards for multistandard calibration: albite (Na), forsterite (Mg), topaz (F), microcline (Al, Si and K) andradite (Ca and Fe), vanadinite (Cl and V), $MnTiO_3$ (Ti and Mn), Cr_2O_3 (Cr) and NiO (Ni). The following parameters were used: accelerating voltage of 15 kV, sample current of 10 nA, beam diameter of 1 µm, and a counting time on the peak of 10 s. Optical microscope images from the CCD video camera and backscattered electron images from SEM were used for selecting analysis spots and for avoiding mineral inclusions.

Reflectance spectroscopy was performed for 88 samples of different lithotypes, using a FieldSpec4® Standard Resolution spectroradiometer (Analytical Spectral Devices) from the University of Campinas (UNICAMP). The spectroradiometer records spectra over 2,151 channels, with wavelengths ranging from 350 to 2,500 nm, comprising the VNIR (350-1,000 nm) and SWIR ranges (1,000-2,500 nm). The spectral sampling (bandwidth) is 1.4 nm for the 350-1,000 nm range, and 1.1 nm for 1,001-2,500 nm (Malvern Panalytical 2020). A contact probe with an internal light source and a 20 mm spot size was used, and a white reference (Spectralon®) was employed for the instrument calibration. The samples were measured at least three times and an average reflectance spectrum was calculated for each sample.

The continuum removal technique (hull quotient) was applied for highlighting the absorption features, providing better visualization of the shape, symmetry, and depth of the absorption features centered at specific wavelengths. This technique consists of normalizing the reflectance spectrum using a mathematical function that defines a convex hull, which fits the spectrum curve. The continuum removal is the ratio of the reflectance values by the continuum line (Clark & Roush 1984, Clark et al. 2003).

The Paraná emerald deposit

In the Pitombeiras mine, the basement rocks are grey-colored biotite gneiss of the Caicó Complex, fine- to medium-grained, with a protomylonitic to mylonitic texture reflecting the intense deformation of the Portalegre ductile strike-slip shear zone. The mylonitic gneisses host lenses of mafic schists, commonly phlogopite schists and actinolite-phlogopite schists, that occur as vertical to sub-vertical bodies within the mylonitic foliation with a NE-SW trend, varying from N15E to N70E (Figure 2a).

The schists are metric-sized, greenish-black colored, fine- to medium-grained, with a lepidoblastic or nematolepidoblastic texture. They host several recrystallized veins and veinlets with granitic compositions and aplitic to pegmatitic textures. These granitic bodies occur as small boudins composed of quartz ±

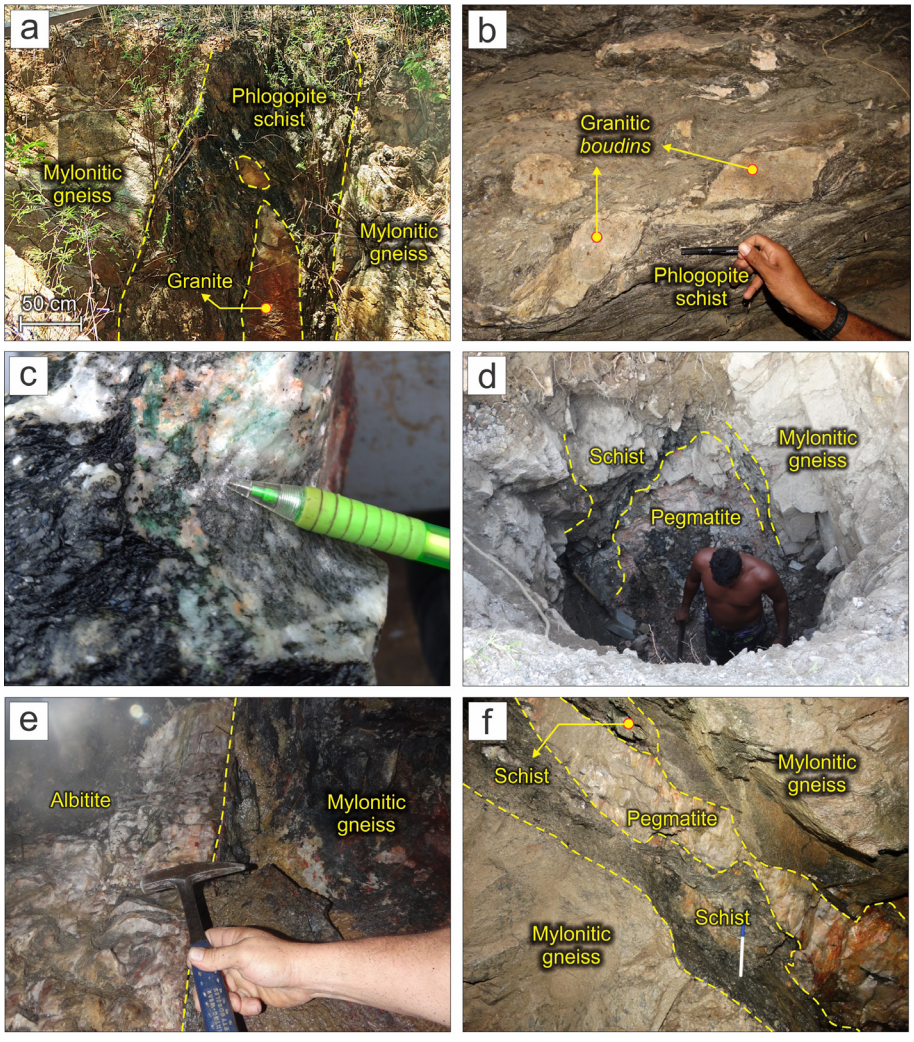

Figure 2. General geological aspects of the Paraná deposit. (a) Vertical to subvertical phlogopite schist within the mylonitic gneiss of the Caicó Complex in Pitombeiras mine. (b) Granitic *boudins* within the schist on a gallery wall at Pitombeiras mine. (c) Emerald crystals at the contact between phlogopite schist and a deformed granitic vein. (d) Phlogopite schist inserted in mylonitic gneiss, displaying a meter-sized deformed pegmatite *boudin* in its core at Pitombeiras mine. (e) Contact between albitite dike and basement mylonitic gneiss on a gallery wall at Pitombeiras mine. (f) Phlogopite schist interleaved with boudinated pegmatite within mylonitic gneisses on the gallery wall at Aroeira mine.

potassium feldspar ± plagioclase, and minor biotite (Figure 2b). Emerald crystals are found (i) within the schistosity planes, (ii) inside the small granitic bodies, or (iii) at the schist-vein contact (Figure 2c). At the regional scale, several granite pegmatites occur along the Portalegre Shear System. In the Pitombeiras region, centimeter- to meter-sized granite pegmatites occur as lenses and veins in association with the emerald-bearing schists (Figure 2d). These pegmatites are often composed of massive potassium feldspar with minor quartz and muscovite, and rarely garnet. Additionally, in the main Pitombeiras shaft, a meter-sized albitite dike occurs adjacent to the basement gneisses (Figure 2e) and the host schists. These albitites are tabular sheared pegmatite bodies, composed of albite and minor pale green muscovite.

In the Aroeiras region, the emerald has been mined within a single shaft, specifically from a gallery 16 meters deep. The phlogopite schist is N30E trending with a dip varying from 60° to 24° to SE and occurs interleaved with quartz-feldspar pegmatite that sometimes seems boudinated. Strongly fractured biotite gneisses of the Caicó Complex host both pegmatite and schist (Figure 2f).

Petrography

Most of the basement rocks are biotite gneisses with protomylonitic to mylonitic textures. On the other hand, the schists can be petrographically divided into three types: phlogopite schist, actinolite-phlogopite schist, and rare phlogopite-phengite schist. No significant differences between samples from the Pitombeiras and Aroeira mines were recorded, although phlogopite-phengite schists were found exclusively outcropping near the main Pitombeiras shaft. The igneous bodies that occur as dikes, veins and veinlets comprise fundamentally quartz and/or feldspar compositions to alkali feldspar granites.

Basement mylonitic gneisses

The basement rocks are essentially plagioclase-rich protomylonitic to mylonitic biotite gneisses with granoblastic or granolepidoblastic textures. Microcline megacrysts characterize some local porphyroclastic textures. The main mineralogy consists of plagioclase (average 57%), microcline (average 14%), quartz (average 13%) and biotite (average 11%). Epidote, allanite, titanite, apatite, and opaque minerals are minor minerals and can represent until 5% of the average modal composition. Few samples also show rare hornblend crystals.

The plagioclase crystals are anhedral to subhedral and typically twinned on the albite law. Altered plagioclases are very common, with sericite formation along the twinning planes (Figure 3a). Anhedral microcline with tartan twinning and perthitic microcline can occur as megacrysts presenting plagioclase with myrmekite around its edges. The interstitial quartz crystals are anhedral with undulatory extinction or vermicular forming myrmekite intergrowths (Figure 3b).

Biotite occurs as oriented subhedral lamellar crystals and shows pleochroism from greenish-brown to pale yellowish-brown. The minor minerals are titanite, apatite, and allanite, which are anhedral to subhedral, with the allanite showing epidote rims and anomalous interference colors due to metamictization (Figure 3c). Epidote varies from small euhedral crystals to anhedral crystals when bordering allanite cores. The opaque minerals show subhedral irregularly shaped rhomb-like sections. Hornblende is rare and occurs as euhedral to subhedral crystals with dark green to

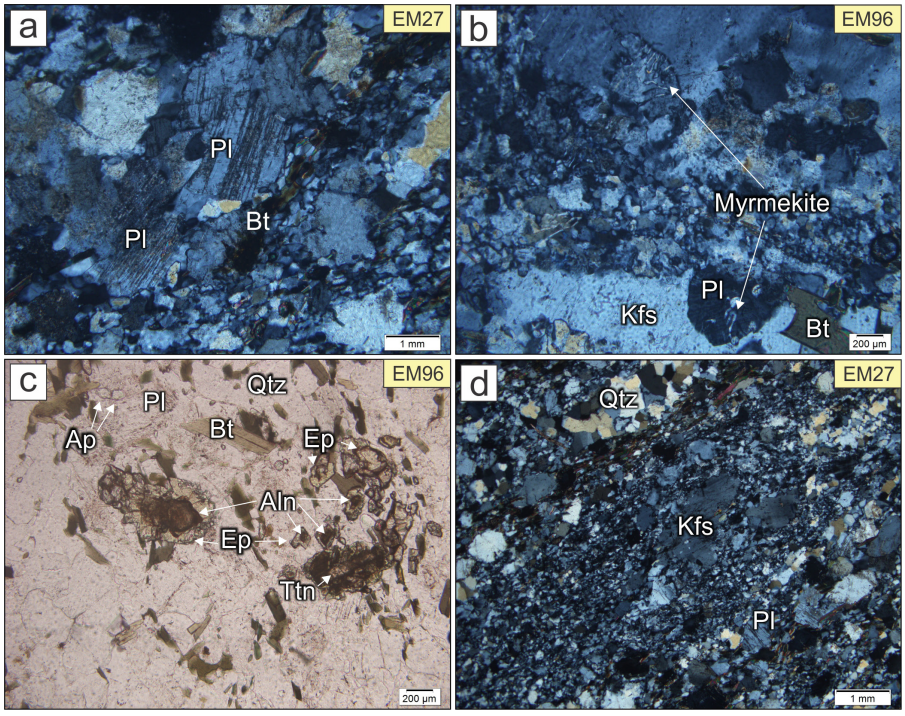

Figure 3. Petrographic features of the basement mylonitic gneisses in Paraná deposit. (a) Plagioclase crystals with sericitization along the twinning plane (NX). (b) Myrmekitic intergrowth at the contact between potassium feldspar and plagioclase (NX). (c) Metamitic allanite with epidote rims in biotite-gneiss (N//). (d) Mylonite with intense recrystallization and formation of quartz and feldspar neoblasts (NX). Transmitted light. NX: crossed nicols; N//: parallel nicols; Aln: allanite; Ap: apatite; Bt: biotite; Ep: epidote; Kfs: potassium feldspar; Pl: plagioclase; Qtz: quartz; Ttn: titanite.

bluish-green colors; sections with two cleavage traces are common.

Mylonitic to protomylonitic facies are characterized by quartz and feldspar neoblasts (Figure 3d). Recrystallization and neoblast formation through subgrain rotation are also frequent.

Phlogopite schists

The phlogopite schists are black colored, fine- to coarse-grained, with texture ranging from lepidoblastic to granolepidoblastic. These schists are composed of phlogopite (Figure 4a), making up about 75% of the total volume, and subordinate quartz, microcline, and plagioclase, which can occur as sigmoids with protomylonitic texture due to intense recrystallization and subgrain formation (Figure 4b). Minor minerals are apatite and rare emerald crystals. The phlogopite crystals are brown to yellow colored and euhedral to subhedral in shape. Quartz, microcline and plagioclase occur in variable proportions but, generally, represent 20-25% of the total volume. Quartz is anhedral with undulatory extinction and often occurs as subgrains. Microcline and plagioclase are anhedral and may be present as coarse crystals with lobe-shaped grain boundary and intense recrystallization at the edges. Apatite exhibits subhedral shape in prismatic and basal sections (Figure 4a). The emerald is subhedral and occurs mainly as basal sections oriented parallel to the schistosity (Figure 4c).

Actinolite-phlogopite schists

The actinolite-phlogopite schists are greenish-black colored, medium- to coarse-grained, with nematolepidoblastic texture. The main mineralogy is phlogopite and actinolite with interstitial quartz and feldspar. Minor minerals are apatite, titanite, and allanite. A few samples also show epidote and emerald as minor constituents. In general, actinolite-phlogopite schists show intrafolial folds and crenulation cleavage in the form of *chevron* folds, evidenced

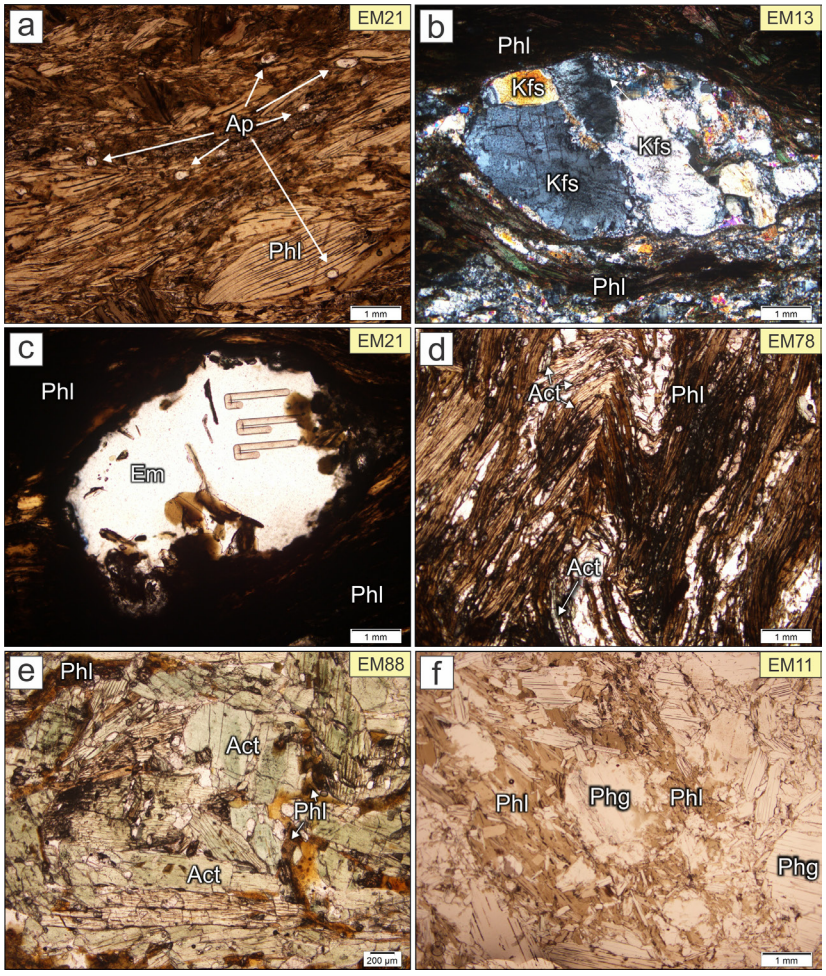

Figure 4. Petrographic features of the schist in Paraná deposit. (a) General aspect of the phlogopite schist (N//). (b) Recrystallization at the borders of sigmoidal feldspar within the phlogopite schist (NX). (c) Emerald crystal within the phlogopite schist (N//). The L-shaped structures are the laser path after laser ablation inductively coupled plasma mass spectrometry (*cf.* Araújo Neto et al. 2019). (d) *Chevron* folds in actinolite-phlogopite schist (N//). (e) Relic phlogopite crystals in actinolite-phlogopite schist (N//). (f) Relic phlogopite crystals in phengite-phlogopite schist (N//). Transmitted light. NX: crossed nicols; N//: parallel nicols; Act: actinolite; Ap: apatite; Em: emerald; Kfs: potassium feldspar; Phg: phengite; Phl: phlogopite.

by deformed phlogopite lamellae with symmetrical limbs (Figure 4d).

There is great variation in the phlogopite and actinolite proportions in each sample. The average content of phlogopite is 54%, with a 16-76% range. Phlogopite crystals are eu- to subhedral, with pale yellow to brown color. Actinolite content averages 24% (3-62%) and comprises euhedral to subhedral prismatic crystals with a faint pleochroism (pale green to colorless), which suggests low Fe contents. Some actinolites show relic phlogopite crystals (Figure 4e). Quartz and feldspars represent about 21% of the total volume; they are anhedral and occur as stretched or minute grains due to recrystallization. Weathered samples often show sericitized alkali feldspar. Apatite occurs as short and prismatic subhedral crystals. Titanite and allanite are rare and anhedral.

Phlogopite-phengite schists

The phlogopite-phengite schists are relatively rare rocks, fine- to coarse-grained, with lepidoblastic texture. Phengite, phlogopite, quartz, and feldspar are the main minerals. Phengite is anhedral, colorless and comprises about 57% of the rock. Some relic phlogopite crystals are observed (Figure 4f). The phlogopite is subhedral, brown to pale yellow colored, representing about 34% of the volume of the rock. Quartz and feldspar are anhedral and represent 9% average of the total volume.

Dikes, veins, and veinlets

These rocks comprise quartz, potassium feldspar, and plagioclase, and can range from pure quartz compositions to granitic ones or even plagioclase dikes (albitites, Figure 5a). They are grouped here due to their few mineralogical variations, leucocratic and acidic natures. The minor minerals are frequently biotite and muscovite, and/or emerald in some cases (Figure 5b), associated with quartz-feldspar *boundins* and veinlets within phlogopite schists. Garnet is rare and can be observed in some potassium feldspar veins (Figure 5c) or in the albitite. In common, these dikes, veins and veinlets often contain altered feldspar (Figure 5d) and protomylonitic texture represented by recrystallization and grain boundary migration of quartz and feldspar (Figure 5e and 5f).

Whole-rock geochemistry

The whole-rock geochemistry analyses of four samples of the phlogopite schist are shown in Table I.

The SiO_2 contents are between 45.67 and 52.36 wt.%, showing the basic nature of the host schist. They present high Al_2O_3 (11.03-14.58 wt.%), as well as MgO (12.90-14.55 wt.%) and Fe_2O_3 (7.51-10.84 wt.%), followed by K_2O (5.52-9.64 wt.%), CaO (0.89-4.50 wt.%) and Na_2O (0.49-2.00 wt.%). The samples also show P_2O_5 concentrations ranging from 0.55 to 1.11 wt.%. Chromium contents are constantly low, ranging from 0.111 to 0.141 wt.%.

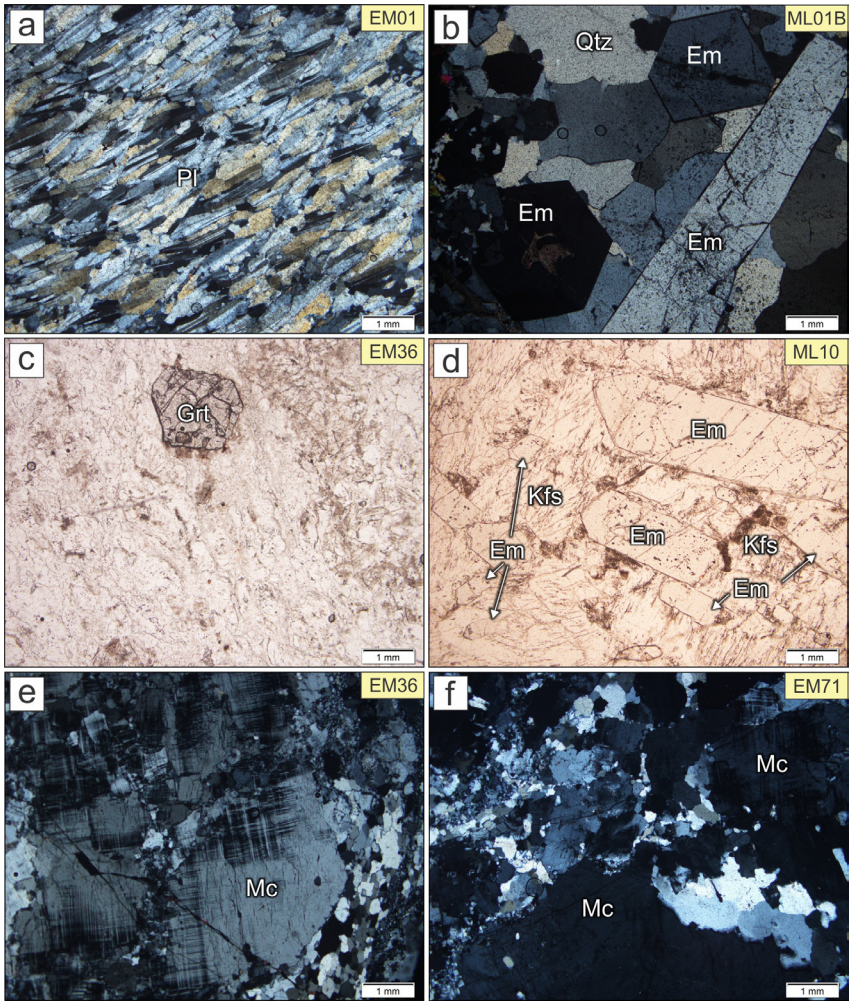

Figure 5. Petrographic features of acidic dikes, veins and veinlets in Paraná deposit. (a) Oriented plagioclase crystals in albitite (NX). (b) Emerald basal and prismatic sections in a quartz vein (NX). (c) Garnet in granitic aplite vein (N//). (d) Vein containing altered potassium feldspar and prismatic idiomorphic emerald crystals (N//). (e, f) Microcline megacrystals exhibiting recrystallization through the grain boundary migration (NX). Transmitted light. NX: crossed nicols; N//: parallel nicols; Em: emerald; Grt: garnet; Kfs: potassium feldspar; Mc: microcline; Pl: plagioclase; Qtz: quartz.

Table I. Whole-rock geochemistry for phlogopite schists of Paraná emerald deposit.

Sample (Locality)	EM21 (Pitombeiras)	EM86 (Pitombeiras)	EM90 (Pitombeiras)	EM114 (Aroeira)
SiO_2 (wt.%)	45.67	48.46	52.36	49.35
TiO_2	0.58	0.70	0.70	0.49
Al_2O_3	14.20	13.50	11.03	14.58
Fe_2O_3*	10.84	8.07	7.83	7.51
MgO	14.55	12.90	12.91	12.94
CaO	0.89	2.68	4.50	1.76
Na_2O	0.49	1.08	1.02	2.00
K_2O	9.64	7.09	5.52	7.84
P_2O_5	0.55	1.11	1.09	0.75
MnO	0.18	0.13	0.13	0.13
Cr_2O_3	0.139	0.111	0.141	0.124
LOI	1.5	3.4	2.0	1.7
Sum	99.23	99.23	99.23	99.17
Ba (ppm)	1,206	1,936	1,608	2,154
Ni	633	456	460	512
Be	300	55	99	124
Co	46	46	45	41
V	86	95	110	80

LOI = loss on ignition; * total iron presented as Fe_2O_3.

Beryllium contents average 144.5 ppm but reach up to 300 ppm in sample EM21, which contains millimetric emerald crystals.

Mineral chemistry

Micas

Several dark-colored and light-colored mica crystals were analyzed by EPMA from six samples of phlogopite schist, one sample of phlogopite-phengite schist, and one sample of albitite (Tables II and III).

In the emerald-hosting schists from Paraná Deposit, the dark-colored micas are phlogopite and ferroan phlogopite, according to the octahedral Fe_{tot}+Mn+Ti-Al^{VI} versus octahedral Mg-Li binary diagram proposed by Tischendorf et al. (2001) (Figure 6). These trioctahedral micas contain 38.96 to 41.38 wt.% SiO_2, 12.40 to 13.67 wt.% Al_2O_3, and 9.93 to 10.17 wt.% K_2O. The content of FeO and MgO ranges from 9.72 to 13.28 wt.%, and 15.23 to 18.72 wt.%, respectively, with $Fe^{2+}/(Fe^{2+}+Mg)$ ratios ranging from 0.23 to 0.32. Fluoride has high average values, between 2.55 and 6.30 wt.%. We estimated Li_2O wt.% from Tischendorf et al. (1999) empirical equation

Table II. EPMA average chemical composition for trioctahedral micas of Paraná emerald deposit.

Sample Rock	EM04 Phl schist	EM11 Phl-Phg schist	EM21 Phl schist	EM82 Phl schist	ML08 Phl schist	ML09A Phl schist	ML09B Phl schist
SiO_2 (wt.%)	39.81	41.38	39.40	39.51	38.96	39.97	40.66
TiO_2	0.74	0.57	0.75	1.01	0.81	1.10	0.92
Al_2O_3	12.40	13.67	13.20	13.15	13.25	12.95	13.28
FeO*	10.04	9.72	10.69	13.28	10.13	10.44	10.07
MnO	0.20	0.41	0.18	0.24	0.15	0.67	0.76
MgO	18.32	15.23	16.96	15.66	18.72	15.96	16.18
CaO	0.04	0.00	0.01	0.00	0.02	0.02	0.02
Na_2O	0.07	0.08	0.14	0.07	0.13	0.14	0.20
K_2O	10.10	10.17	10.04	9.97	9.93	10.00	9.97
F	4.77	6.30	4.72	4.20	2.55	4.93	4.97
Cl	0.01	0.01	0.05	0.01	0.00	0.02	0.09
Cr_2O_3	0.15	0.05	0.18	0.14	0.25	0.14	0.06
NiO	0.08	0.06	0.10	0.03	0.07	0.09	0.07
Li_2O**	0.02	0.05	0.03	0.04	0.02	0.04	0.04
$H_2O^{\dagger}$	1.70	0.99	1.69	1.96	2.77	1.59	1.60
Subtotal	98.46	98.67	98.15	99.26	97.77	98.06	98.89
O=F,Cl	2.01	2.65	2.00	1.77	1.07	2.08	2.11
Total	96.45	96.02	96.16	97.49	96.70	95.98	96.78
Si (apfu)	6.024	6.246	5.996	5.989	5.873	6.089	6.121
Al^{IV}	1.976	1.754	2.004	2.011	2.127	1.911	1.879
Al^{VI}	0.236	0.680	0.364	0.338	0.227	0.414	0.478
Ti	0.084	0.065	0.086	0.115	0.092	0.126	0.104
Cr	0.018	0.005	0.022	0.016	0.030	0.017	0.008
Fe^{2+}	1.270	1.227	1.361	1.684	1.277	1.330	1.267
Mn	0.025	0.053	0.024	0.031	0.020	0.086	0.097
Mg	4.132	3.428	3.847	3.539	4.206	3.623	3.630
Ni	0.010	0.008	0.012	0.003	0.008	0.011	0.009
Li**	0.015	0.028	0.020	0.026	0.013	0.025	0.024
Ca	0.007	0.001	0.002	0.000	0.003	0.002	0.003
Na	0.021	0.023	0.041	0.019	0.038	0.041	0.057
K	1.949	1.958	1.948	1.928	1.910	1.944	1.915
$OH^{\dagger}$	1.714	0.993	1.718	1.985	2.784	1.617	1.610
F	2.282	3.006	2.271	2.012	1.215	2.377	2.368
Cl	0.004	0.002	0.012	0.003	0.001	0.006	0.022
$Fe^{2+}/(Fe^{2+}+Mg)$	0.235	0.264	0.261	0.322	0.233	0.269	0.259

Average of at least three analyzed micas per sample. Stoichiometry based on 22 oxygens. apfu: atoms per formula unit; *total iron presented as FeO; **Li_2O calculated through the equation: Li_2O = 2.1/(0.356+MgO) – 0.088 (Tischendorf et al. 1999); † H_2O obtained by stoichiometry, assuming OH + F + Cl = 4 apfu. Phg: phengite; Phl: phlogopite.

[Li_2O = 2.1/(0.356 + MgO) - 0.088], validated for micas with MgO contents from 0 to 23 wt.%. The calculated average Li contents are low, ranging from 0.02 to 0.05 wt.% LiO_2 (Table II).

The light-colored dioctahedral micas from the phlogopite-phengite schist are ferroan muscovites (Figure 7), a nomenclature approved by the International Mineralogical Association

Table III. EPMA average chemical composition for dioctahedral micas of Paraná emerald deposit.

Sample Rock	EM11 Phlogopite-phengite schist	EM01 Muscovite albitite
SiO_2 (wt.%)	46.60	45.38
TiO_2	0.32	0.03
Al_2O_3	26.26	36.54
FeO*	3.45	0.49
MnO	0.13	0.18
MgO	4.02	0.01
CaO	0.02	0.00
Na_2O	0.25	0.43
K_2O	10.49	10.36
F	2.79	0.15
Cl	0.01	0.01
Cr_2O_3	0.10	0.03
NiO	0.03	0.01
Li_2O**	0.79	0.00
$H_2O^{\dagger}$	2.97	4.37
Subtotal	98.23	98.00
O=F,Cl	1.18	0.06
Total	97.05	97.94
Si (apfu)	6.497	6.123
Al^{IV}	1.503	1.877
Al^{VI}	2.814	3.933
Ti	0.034	0.003
Cr	0.011	0.004
Fe	0.402	0.055
Mn	0.015	0.021
Mg	0.835	0.002
Ni	0.003	0.001
Li**	0.445	0.000
Ca	0.003	0.001
Na	0.067	0.112
K	1.865	1.782
$OH^{\dagger}$	2.766	3.936
F	1.231	0.063
Cl	0.003	0.001

Average of six and nine analyzed micas for sample EM11 and EM01, respectively. Stoichiometry based on 22 oxygens. apfu: atoms per formula unit; *total iron presented as FeO; **Li_2O calculated through the equation: Li_2O = (0.31134*F) – 0.075895 (Monier & Robert 1986). † H_2O obtained by stoichiometry, assuming OH + F + Cl = 4 apfu.

(IMA) for white micas with Si in excess and fairly large amounts of Mg and Fe, which was previously and still widely known as phengite. The ferroan muscovite crystals contain 46.60 wt.% SiO_2 and 10.49 wt.% K_2O (Table III). As expected, the aluminum content is very low compared to typical muscovite, averaging 26.26 wt.% Al_2O_3, which is followed by a significant increase in FeO (3.45 wt.%) and MgO (4.02 wt.%) average concentrations. The fluoride content is in the range of those of the phlogopite crystals, averaging 2.79 wt.%.

Pale green mica appears as an accessory mineral in albitite dikes. Its major element chemistry resembles those of pure muscovite (Figure 7), with average SiO_2, Al_2O_3 and K_2O of 45.38, 36.54, and 10.36 wt.%, respectively. It has 0.49 wt.% FeO, 0.43 wt.% Na_2O, 0.18 wt.% MnO, and a very low F content (0.15 wt.%). The average values of MgO, Cr_2O_3, NiO, and TiO_2 are all below 0.1 wt.% (Table III).

Amphiboles

One thin section of a representative amphibole-bearing schist (sample EM88) from the Pitombeiras mine was also chemically analyzed by EPMA (Table IV). The studied amphibole crystals are magnesium-enriched calcium amphiboles, containing, on average, 57.00 wt.% SiO_2, 19.69 wt.% MgO, 12.75 wt.% CaO, 6.44 wt.% FeO, 2.13 wt.% $H_2O_{(calculated)}$, and 1.03 wt.% Al_2O_3. Other oxides show an average concentration below 1 wt.%.

According to the diagram by Hawthorne et al. (2012) for calcium amphiboles, these magnesium-rich amphiboles are in the field of tremolite (Figure 8). In this case, however, the term “actinolite” is more suitable since it was retained for petrological reasons in the Hawthorne et al. (2012) classification for amphiboles of the tremolite–ferro-actinolite series with a compositional range that extends

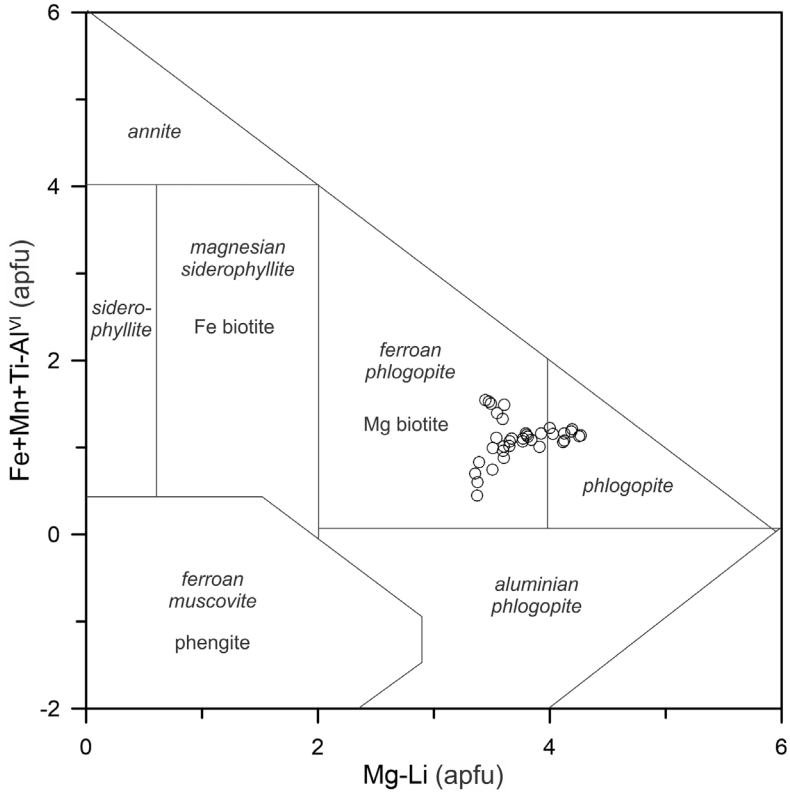

Figure 6. Octahedral Fe_{tot}+Mn+Ti-Al^{VI} versus octahedral Mg-Li for trioctahedral micas. Adapted from Tischendorf et al. (2001). Result of 36 spots analyzed by EPMA. IMA approved nomenclature is in italics.

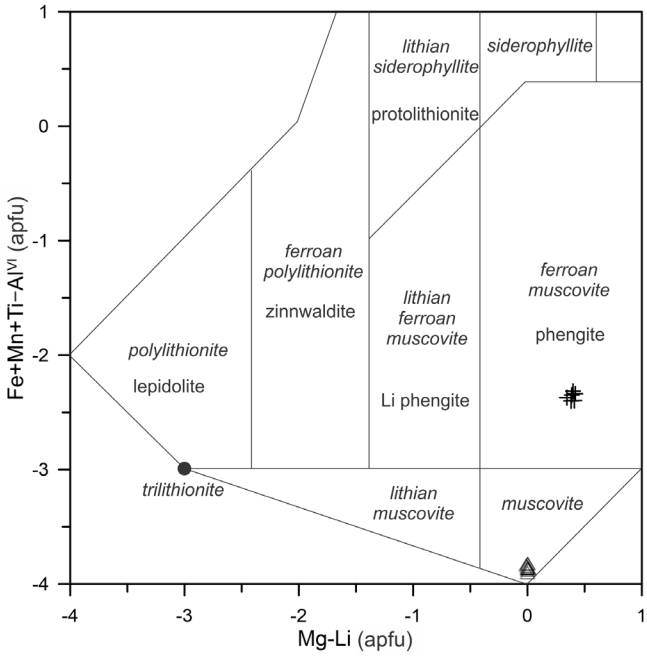

Figure 7. Octahedral Fe_{tot}+Mn+Ti-Al^{VI} versus octahedral Mg-Li for dioctahedral micas. Adapted from Tischendorf et al. (2001). Result of 15 spots analyzed by EPMA. IMA approved nomenclature is in italics. + Sample EM11; Δ Sample EM01.

Table IV. EPMA average chemical composition for amphibole of Paraná emerald deposit.

Sample	EM88		EM88
SiO_2 (wt.%)	57.00	Si (apfu)	7.950
TiO_2	0.05	Al^{IV}	0.050
Al_2O_3	1.03	Al^{VI}	0.120
Cr_2O_3	0.07	Ti	0.005
NiO	0.07	Cr	0.008
FeO*	6.44	Ni	0.008
MnO	0.23	Fe^{2+}	0.751
MgO	19.69	Mn	0.027
CaO	12.75	Mg	4.095
Na_2O	0.23	Ca	1.906
K_2O	0.07	Na	0.062
F	0.04	K	0.013
Cl	0.00		
$H_2O^{\dagger}$	2.13	$OH^{\dagger}$	1.983
Subtotal	99.86	F	0.016
O=F,Cl	0.02	Cl	0.001
Total	99.84	$Mg/(Mg+Fe^{2+})$	0.845

Average of 15 analyzed spots in amphiboles of sample EM88. Stoichiometry based on 24 anions. apfu: atoms per formula unit; *total iron as FeO; † H_2O obtained by stoichiometry, assuming OH + F + Cl = 2 apfu.

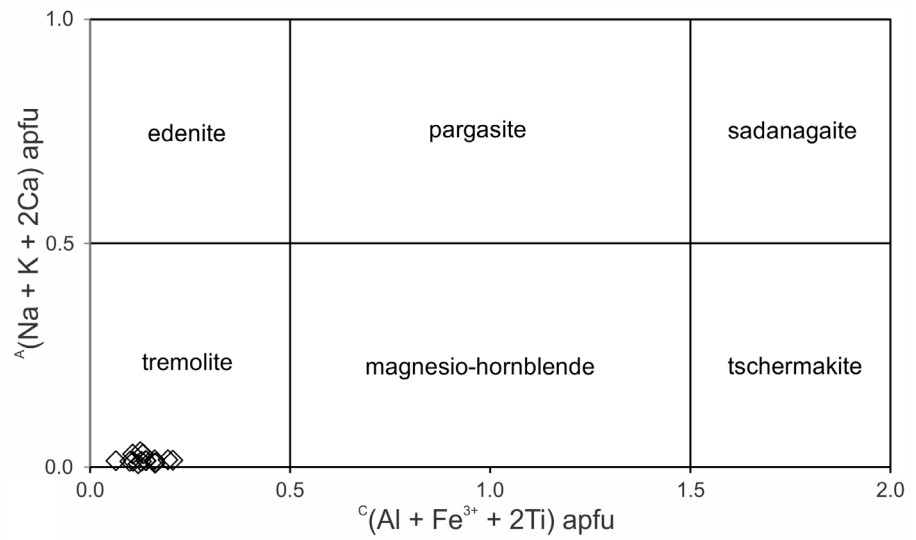

Figure 8. $^{C}(Al + Fe^{3+} + 2Ti)$ versus $^{A}(Na + K + 2Ca)$ diagram for calcium amphiboles. Results of 15 analyzed spots by EPMA. Classification fields after Hawthorne et al. (2012).

from Mg < 4.5 apfu and Fe^{2+} > 0.5 apfu to Mg ≥ 2.5 apfu and Fe^{2+} ≤ 2.5 apfu.

Reflectance spectroscopy

The spectral characterization was carried out using representative samples from the Pitombeiras and Aroeira mines. Phlogopite-, actinolite-phlogopite-, and phlogopite-phengite schists from the Pitombeiras mine show broad absorption features in the VNIR and SWIR range (400-1,600 nm) due to the presence of Fe^{2+} in the structure of ferromagnesian micas and amphiboles. Subtle absorption features at ~900 nm are also attributed to Fe^{2+}, while features near 700 nm are related to Fe^{3+}-Fe^{2+} charge transfer (*cf.* Hunt 1977, Dyar 1990, Pontual et al. 2008) (Figure 9a).

For the Pitombeiras' schists, the SWIR region is marked by a subtle absorption at ~1,395 nm, associated with OH^- and/or water molecular vibrational processes, and an asymmetric absorption feature at 1,910 nm due to the vibration of water molecules (*cf*. Hunt 1977, Clark 1999, Pontual et al. 2008) (Figure 9a). The 2,150 to 2,450 nm range shows the best diagnostic features for each schist type, reflecting the mineralogical composition (Figure 9b). The absorption feature at ~2,250 nm occurs in all schist samples due to Fe-OH vibrational processes in both phlogopite and/or actinolite (Hunt 1977, Clark et al. 1990, Pontual et al. 2008). The phlogopite schists are also marked by absorptions at ~2,330 and ~2,388 nm related to the Mg-OH bond in phlogopite (Clark et al. 1990, Pontual et al. 2008). In the actinolite-phlogopite schists, the spectral signature of actinolite is predominant and it is marked by the double Mg-OH feature at ~2,297 and ~2,320 nm, although a secondary Mg-OH feature at ~2,388 nm can also be observed (Pontual et al. 2008). In the phlogopite-phengite schists both Mg-OH features of phlogopite are masked by the presence of typical phengite Al-OH absorption at ~2,350 nm and 2,450 nm (Scott & Yang 1997). These schists are also marked by an expressive absorption feature at ~2,218 nm associated with Al-OH bonds diagnostic for white micas like phengite (Scott & Yang 1997, Pontual et al. 2008). On the other hand, Al-OH absorption bands can be expected as well in weathered phlogopite schists due to the presence of clay minerals and/or sericite (*e.g.* double OH^- features at ~1,390 and ~1,412 nm, and double Al-OH features at ~2,167 and ~2,208 nm in sample EM21, likely related to the presence of kaolinite; Hunt 1977, Pontual et al. 2008) (Figure 9b).

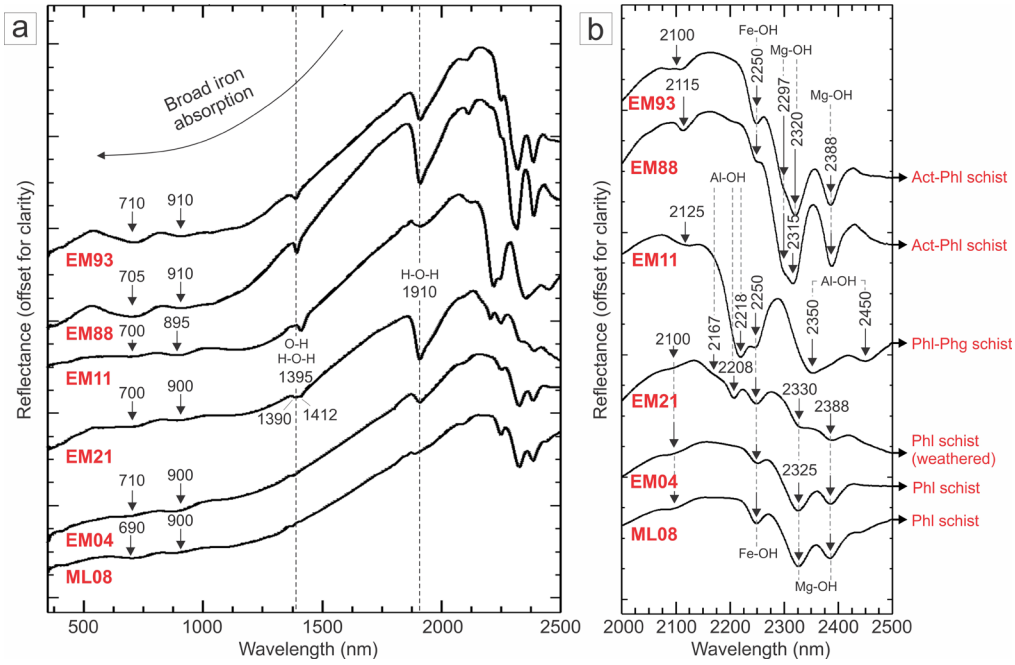

Figure 9. Stacked reflectance spectra of schists from Pitombeiras mine and indication of main absorption features. (a) Absorption features in the VNIR-SWIR range. (b) Detail of absorption features in the SWIR range. Act: actinolite; Phg: phengite; Phl: phlogopite.

Spectral interpretations of other rocks from the Pitombeiras mine show that the broad Fe^{2+} absorption feature of biotite in the VNIR region allows for the swift distinction between biotite gneisses and rocks of essentially quartz-feldspar compositions (Figure 10a). In the SWIR range (Figure 10b), biotite gneisses show absorptions at ~2,250 nm (Fe-OH) and ~2,330 and ~2,384 nm (Mg-OH) related to biotite/phlogopite (Hunt 1977, Clark et al. 1990, Pontual et al. 2008). The absorption feature at ~2,200 nm (Al-OH) is common due to potassium feldspar alteration to sericite or clay minerals (Pontual et al. 2008).

The analysis of an orange-colored potassium feldspar vein shows atypical Al-OH absorption (2,205 nm) and OH^- and/or water absorptions at 1,438 and 1,929 nm (Figure 10b). These absorption features likely originated from alteration processes such as sericitization. In the VNIR region, a deep absorption feature at 440 nm is probably related to the presence of Fe^{3+} in the feldspar crystal structure, which is responsible for the orange color (*cf.* Faye 1969) (Figure 10a).

Also, a sample of muscovite-bearing albitite is marked by the spectral signature of muscovite (Hunt 1977, Pontual et al. 2008), with a deep Al-OH absorption feature at 2,195 nm, and secondary ones at 2,343 and 2,433 nm (Figure 10b). The presence of deep OH^- and/or water absorptions at 1,407 and 1,910 nm suggests a contribution from illite and/or sericite, common products of weathering.

In the Aroeira mine, the spectral analysis of a lithological profile parallel to the dip direction of both schist and pegmatite (Figure 11a), shows the influence of Al-OH, Fe-OH, and Mg-OH absorption features for characterizing the different lithotypes of the emerald deposit. In the SWIR region (Figure 11b), the mylonitic biotite gneiss (sample EM111) shows the relatively deep Fe-OH (~2,250 nm) and Mg-OH (~2,333, ~2,388 nm) absorption features of biotite, and a subtle Al-OH absorption at 2,200 nm which is probably due to some alkali feldspar alteration. This feature at 2,200 nm is deeper in sample EM112, a quartz-feldspar pegmatite near the contact with the biotite gneiss, probably due to a higher concentration of altered alkali feldspar (Figure

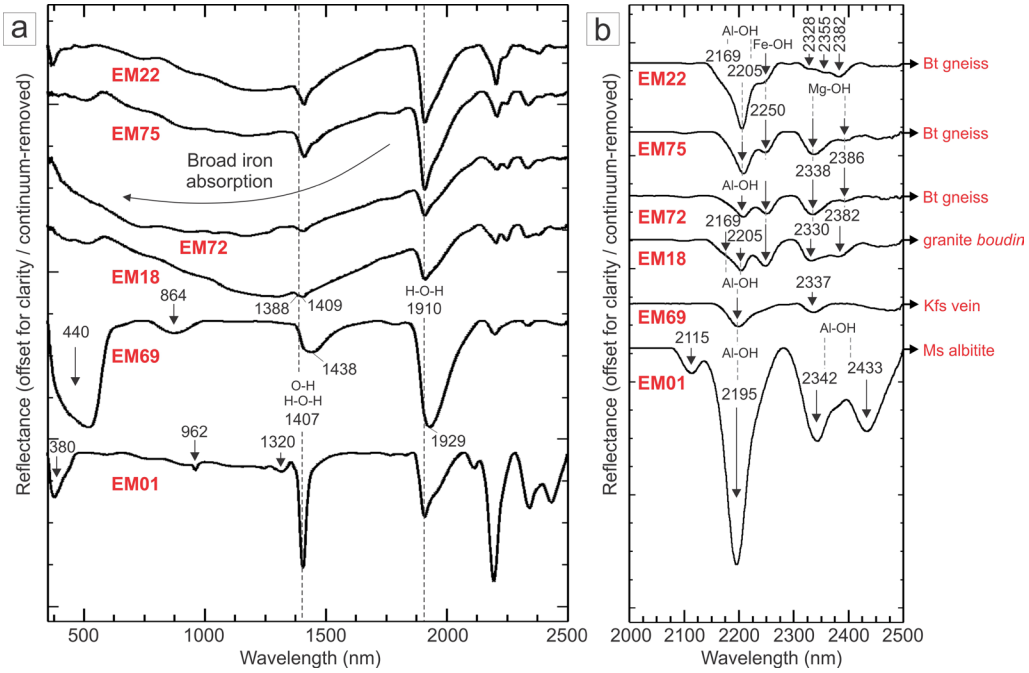

Figure 10. Stacked reflectance spectra of gneisses and acidic rocks from Pitombeiras mine, and indication of main absorption features. (a) Absorption features in the VNIR-SWIR range. (b) Detail of absorption features in the SWIR range. Bt: biotite; Kfs: potassium feldspar; Ms: muscovite.

11b). On the other hand, a quartz-feldspar pegmatite sample (EM113) at the contact with the phlogopite schists, shows a spectral signature dominated by the phlogopite absorption features of Fe-OH and Mg-OH bonds. The Al-OH feature at 2,200 nm disappears in the phlogopite schist (sample EM114) since phlogopite concentrations subdue those of altered feldspar. However, if the phlogopite schist contains alkali feldspar veinlets and/or megacrysts (sample EM115), it may be characterized by well-pronounced absorption features derived from Fe-OH, Mg-OH, and Al-OH molecular vibrational process (Figure 11b).

The emerald-bearing schist spectra

Araújo Neto et al. (2019) previously investigated rough emerald crystals spectra from the Paraná deposit. In brief, these emeralds are marked by Cr^{3+} absorption features in the VNIR range at ~430 nm and ~630 nm, and a broad Fe^{2+} absorption band at ~850 nm. In the SWIR range, the emeralds show water absorption features at ~1,150, ~1,410, ~1,900 nm, and other four non-identified features at 2,072, 2,158, 2,205, and 2,329 nm.

The spectra of emeralds that are within the host schists show a mixture of spectral responses from different minerals (Figure 12). Sample ML01 contains several prismatic emeralds in a quartz-feldspar vein inside the phlogopite schist. Spectral analysis in these crystals shows sharp and well-defined absorptions features typical for the expected emerald spectrum. Nevertheless, if the emerald crystal is hosted within the schist foliation, the Cr^{3+} and water absorptions appear attenuated by the broad absorption of Fe^{2+} in phlogopite. In this case, phlogopite absorption features are well marked at 2,252 nm (Fe-OH), and 2,328 and 2,388 nm (Mg-OH), and the diagnostic emerald features are hard (if not impossible) to distinguish. This attenuation occurs even in large centimetric emerald crystals with few mica flakes at the surface, such as observed in sample ML05 (Figure 12).

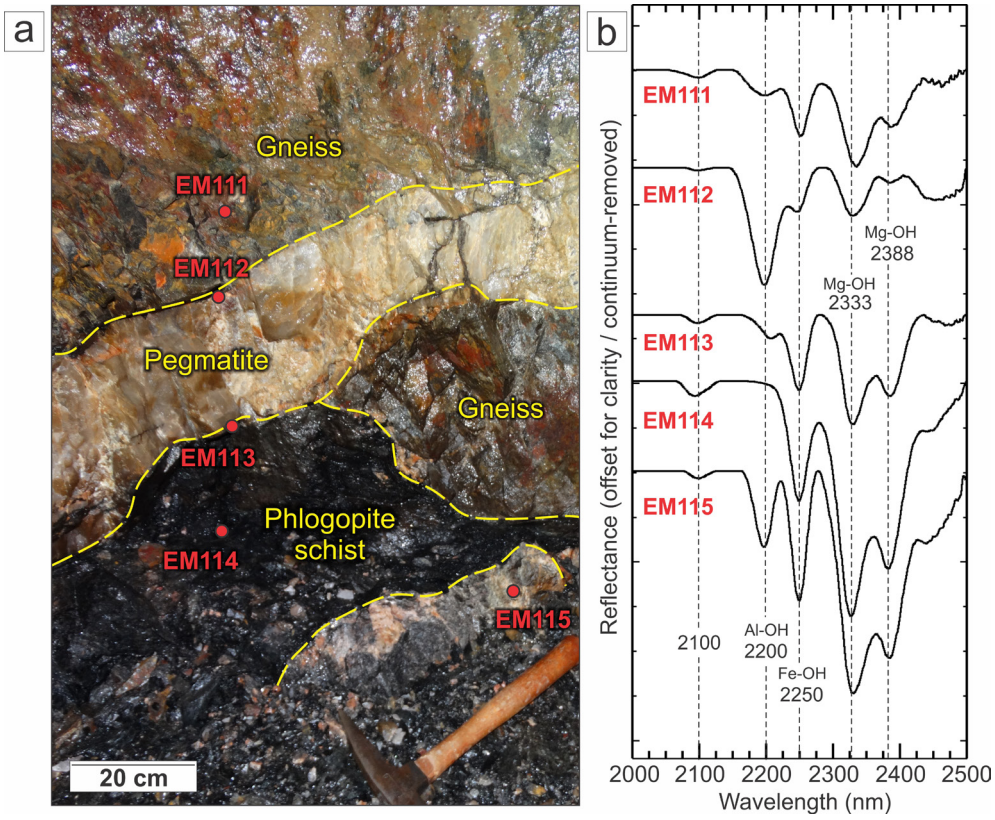

Figure 11. Main spectral responses in a profile sampling at Aroeira mine. (a) Representative lithological profile of the deposit. (b) Detail of absorption features of different rocks in the SWIR range.

DISCUSSION

The emeralds from the Paraná deposit are associated with quartz-feldspar veins and veinlets interleaved with basic schists (average of 48.96 wt.% SiO_2) that are rich in magnesium (average of 13.33 wt.% MgO) and iron (average of 8.56 wt.% FeO). The schist mineralogical composition varies from the common phlogopite schist to actinolite-phlogopite schist, and phlogopite-phengite schist, all hosted by mylonitic gneisses within the Portalegre Shear Zone. The absence of ultrabasic and/or metaultrabasic rocks in this region (*e.g.* dunites, pyroxenites, talc-serpentinites, and serpentinites) suggests that the metabasic lenses of amphibolite, which occur in proximity to the Portalegre Shear Zone, are the best candidates to be the source of iron and chromium in emerald (Souza 2017). This hypothesis is corroborated by the high iron and low chromium and vanadium content in the Paraná phlogopite schists. This pattern is similarly reflected in the emerald crystals of the Paraná deposit, which contains higher Fe, and lower Cr and V in comparison to other deposits associated with ultrabasic rocks (Araújo Neto et al. 2019). However, until the development of this research, the field relations between amphibolite and schist could not be observed since all amphibolite lenses were found a few kilometers far from the Pitombeiras and Aroeira mines.

The pegmatite injections across the Portalegre Shear Zone are probably the source of Be, and the presence of albite-rich pegmatites suggests metasomatic modification (desilication) of previous granitic pegmatites (Walton 2004), with Si leaving the pegmatite to probably form metasomatic schists and the numerous quartz veins. Desilication provides a relative Al enrichment in the pegmatite that results in recrystallization of Al-rich minerals

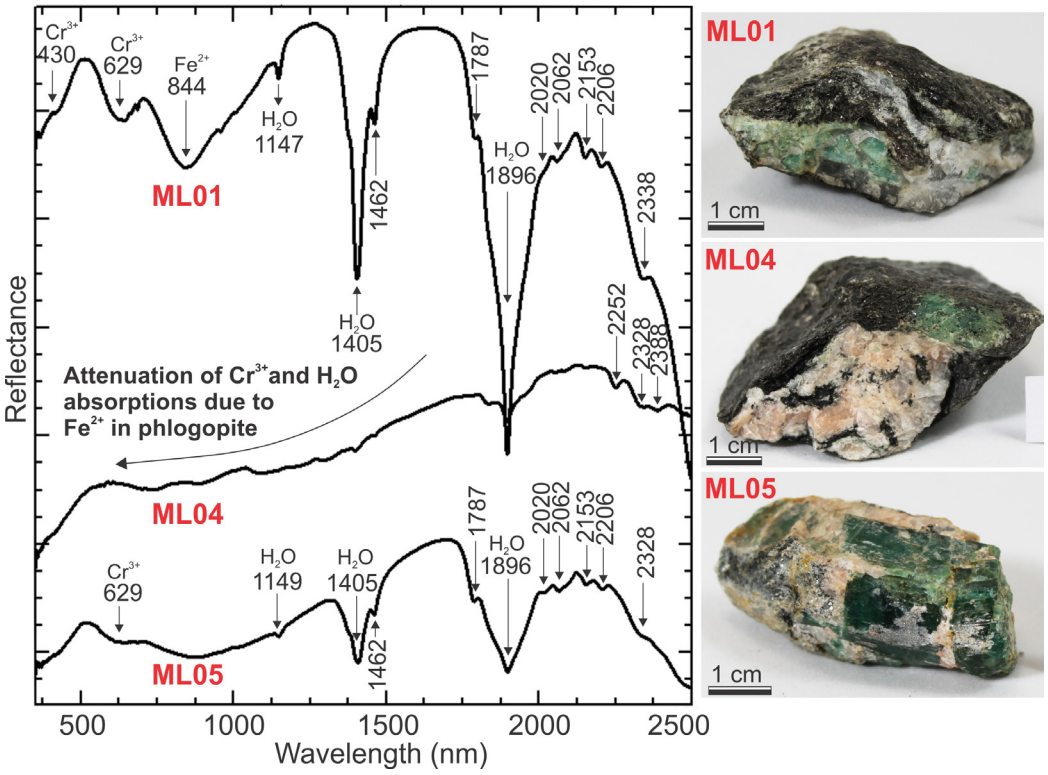

Figure 12. Stacked reflectance spectra of rough emeralds in host rock, and interpretation of main absorption features.

such as muscovite and garnet (Černý 2002). Additionally, the compositional variation of schists, from phlogopite- to phlogopite-phengite- and actinolite-phlogopite schists, with phlogopite relicts in both actinolite and phengite, implies possible variations in the metasomatic process. Nevertheless, the spatial distribution of these schists is not in well-defined zones, but an erratic disposition across the deposit. Emerald crystals are found in both phlogopite and actinolite-phlogopite schist, but so far, no phlogopite-phengite schist has contained emerald.

Reflectance spectroscopy proved to be a powerful tool on the investigation of the different lithotypes that compose the Paraná emerald deposit. Because of its rapid and non-destructive properties, reflectance spectroscopy can quickly distinguish mineralogical variations among basic schist samples. Phlogopite-, phlogopite-phengite-, and actinolite-phlogopite schists can be recognized mainly by distinctive absorption features in the 2,210-2,400 nm spectral range, unveiling both mineralogical content and chemical composition of these rock types (Figure 13a).

The relation between the wavelength of minimum reflectance and the MgO and FeO contents (wt.%) for representative schists is shown in figures 13b and 13c, respectively. The minimum reflectance for phengite-bearing schist is at 2,218 nm (Al-OH), while pure phlogopite schists have the minimum reflectance centered at 2,330 nm (Mg-OH), shifting to 2,325 nm with the increasing of MgO content in phlogopites (Figure 13b). Lastly, the actinolite-bearing schists also have a minimum reflectance associated with Mg-OH vibrational process but centered at 2,315 nm (Figure 13a).

Samples of emerald crystals hosted by schist could not be appropriately identified using reflectance spectroscopy due to the attenuation of the VNIR absorption features of emerald by the broad iron absorption of phlogopite and

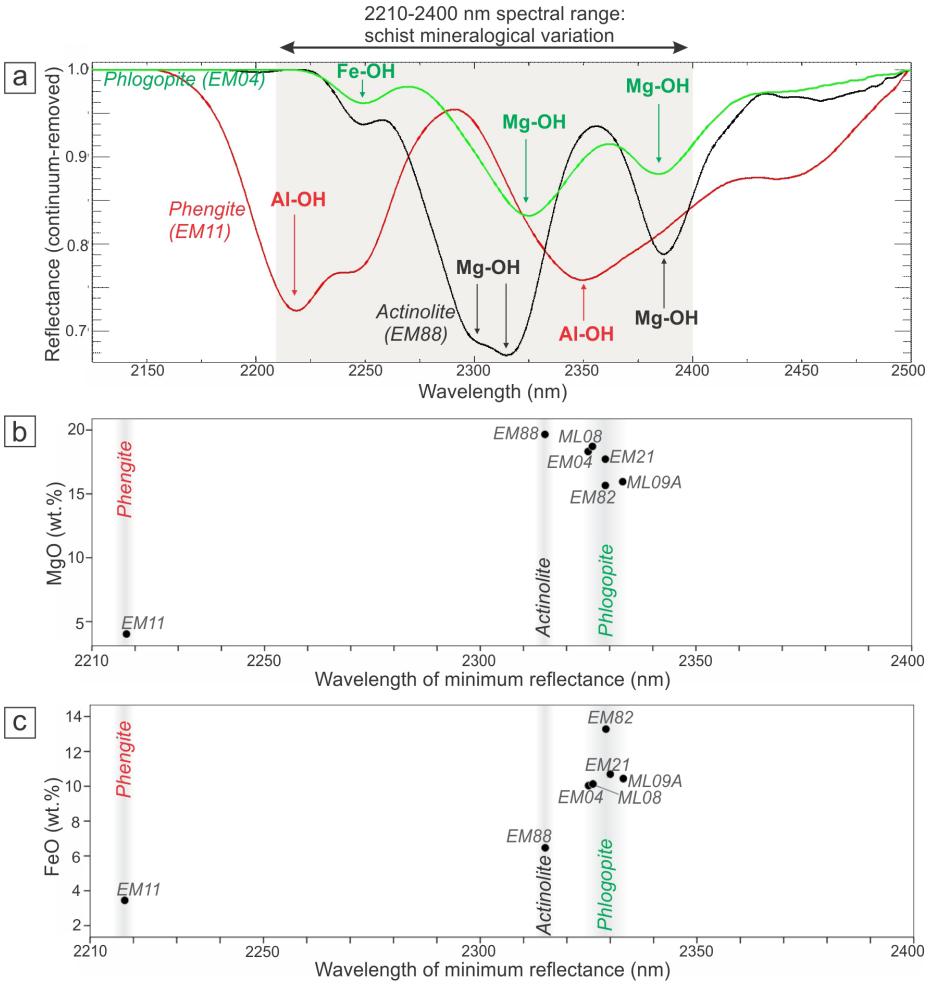

Figure 13. Relation between the wavelength of the minimum reflectance and the MgO and FeO contents (wt.%) for representative schist samples of the Paraná emerald deposit. (a) Representative spectra of schists containing phengite, actinolite and phlogopite. (b) Wavelength of minimum reflectance versus MgO content (wt.%). (c) Wavelength of minimum reflectance versus FeO content (wt.%).

amphibole. This attenuation restricts the role of the point spectral analysis as a prospective tool in the identification of emerald signatures on local and regional scale. However, reflectance spectroscopy can still be used as a prospective tool in the investigation and identification of the host basic schists.

CONCLUSIONS

The geological setting of the Paraná emerald deposit shows characteristic features of the classic schist-type deposit (see Sinkankas 1981, Schwarz 1987, Walton 2004, Groat et al. 2008), with the formation of emerald-bearing quartz-feldspar veins and veinlets hosted in phlogopite- and actinolite-phlogopite schists probably due to metasomatic interaction between granitic pegmatites and (meta)basic/ultrabasic rocks. This interaction and the mobilization of Be and chromophores elements (Cr, V and Fe) most-certainly happened during a Neoproterozoic strike-slip shearing represented by the Portalegre Shear Zone.

The presence of muscovite albitite and the schist compositional variation are indicative of fluid interactions and metasomatic modification (desilicated pegmatites). The uncommon high iron, and low chromium and vanadium content in Paraná schists and emerald crystals, associated with the absence of (meta)ultrabasic rocks in the region suggest a metabasic source of chromophore elements, with the Caicó

amphibolite lenses as the main candidates to be this source.

Despite being an unusual method for emerald exploration, reflectance spectroscopy proved to be useful in the spectral characterization and individualization of the different lithotypes found in the deposit, especially using the SWIR range of 2,200-2,400 nm, where the main mafic minerals show absorption features derived from Al-OH bonds (phengite), and Fe-OH and Mg-OH bonds (phlogopite and actinolite).

Typical potential host rocks such as phlogopite schists and actinolite-phlogopite schists can be readily distinguished using reflectance spectroscopy from sterile rocks like phlogopite-phengite schists even though by visual analysis they are almost identical. Still, the point spectral analysis is not able to fully distinct emerald-bearing phlogopite schists from phlogopite schists without emerald due to masking of emerald absorption features by major phlogopite features. This masking can be surpassed in future evaluations by changing point spectral analysis for hyperspectral imaging.

Notwithstanding this restriction, spectral reflectance studies can be performed by using systematic reflectance and imaging spectroscopy in drill cores, as well as high resolution airborne or orbital optical sensors to target potential host rocks.

Acknowledgments

The authors are grateful to Mr. Luis Amorim and all the crew of Mineração Limeira Comércio, Exportação e Importação for providing support to our research in field studies. We would like to express our gratitude to Professor Dr. Nilson Botelho (University of Brasília, Brazil) for the EPMA facilities. The reflectance spectroscopy was done in the Geoscience Institute of UNICAMP thanks to Professor Dr. Carlos R. de Souza Filho, Dr. Rebecca Scafutto and Dr. Rosa Pabón. We thank Coordenação de Aperfeiçoamento de Pessoal de Nível Superior (CAPES) for the scholarship granted to José Ferreira de Araújo Neto, Igor Manoel Belo de Albuquerque e Souza and Glenda Lira Santos. The authors also thank the reviewers for their significant contributions to this work.

REFERENCES

ALMEIDA FFM, HASUI Y, BRITO NEVES BB & FUCK RA. 1981. Brazilian Structural Provinces: an introduction. Earth-Sci Rev 17(1-2): 1-29.

ANGELIM LAA. 2006. Geologia e Recursos Minerais do Estado do Rio Grande do Norte. Escala 1:500.000. Recife: CPRM/FAPER.

ARAÚJO NETO JF, BARRETO SB, CARRINO TA, MÜLLER A & SANTOS LCML. 2019. Mineralogical and gemological characterization of emerald crystals from Paraná deposit, NE Brazil: a study of mineral chemistry, absorption and reflectance spectroscopy and thermal analysis. Braz J Geol 49(3): 1-15.

ARAÚJO NETO JF, SANTOS GL, SOUZA IMBA, BARRETO SB, SANTOS LCML, BEZERRA JPS & CARRINO TA. 2018. Integration of remote sensing, airborne geophysics and structural analysis to geological mapping: a case study of the Vieiropolis region, Borborema Province, NE Brazil. Geol USP Sér Cient 18(3): 89-103.

BARRETO SB, MÜLLER A, ARAUJO NETO JF, BEZERRA JPS, SOUZA IMBA, FRANÇA RHM & SANTOS LCML. 2016. Vieirópolis Pegmatite Field, Northwest of Paraíba State, Brazil: New Occurrences of Amazonite Pegmatites. In: Jacobson MI (Ed), Second Eugene E. Foord Pegmatite Symposium: Abstracts, Short Papers, Posters and Program, Denver, Friends of Mineralogy, Colorado Chapter, p. 24-26.

BEDELL RL, CRÓSTA AP & GRUNSKY E. 2009. Remote Sensing and Spectral Geology. Reviews in economic geology 16. SEG, 266 p.

BEURLEN H, BARRETO SB, MARTIN R, MELGAREJO J, SILVA MRR & SOUZA NETO JA. 2009. The Borborema Pegmatite Province, NE-Brazil revisited. Est Geol 19(2): 62-69.

BRITO NEVES BB, FUCK RA & PIMENTEL MM. 2014. The Brasiliano collage in South America: a review. Braz J Geol 44(3): 493-518.

BRITO NEVES BB, SANTOS EJ & VAN SCHMUS WR. 2000. Tectonic History of the Borborema Province. In: Cordani UG, Milani EJ, Tomaz Filho A and Campos DA (Eds), Tectonic Evolution of South America, 31st International Geological Congress, Rio de Janeiro, p. 151-182.

CARRINO TA, CRÓSTA AP, TOLEDO CLB & SILVA AM. 2018. Hyperspectral remote sensing applied to mineral exploration in southern Peru: a multiple data integration

approach in the Chapi Chiara gold prospect. Int J Appl Earth Obs 64: 287-300.

ČERNÝ P. 2002. Mineralogy of Beryllium in Granitic Pegmatites. In: Grew ES (Ed), Beryllium - Mineralogy, Petrology and Geochemistry. Rev Mineral Geochem 50: 405-444.

CLARK RN. 1999. Spectroscopy of rocks and minerals, and principles of spectroscopy. In: Rencz AN (Ed). Manual of remote sensing. Remote Sensing for the Earth Science, 3, New York, J Wiley & Sons, p. 3-58.

CLARK RN, KING TVV, KLEJWA M, SWAYZE GA & VERGO N. 1990. High spectral resolution reflectance spectroscopy of minerals. J Geophys Res 95(B8): 12653-12680.

CLARK RN & ROUSH TL. 1984. Reflectance spectroscopy: quantitative analysis techniques for remote sensing applications. J Geophys Res 89(B7): 6329-6340.

CLARK RN, SWAYZE GA, LIVO KE, KOKALY RF, SUTLEY SJ, DALTON JB, MCDOUGAL RR & GENT CA. 2003. Imaging spectroscopy: Earth and planetary remote sensing with the USGS Tetracorder and expert systems. J Geophys Res 108(12): 1-44.

DYAR MD. 1990. Mossbauer spectra of biotite from metapelites. Am Mineral 75: 656-666.

FAYE GH. 1969. The optical absorption spectrum of tetrahedrally bonded Fe3+ in orthoclase. Can Mineral 10: 112-117.

GIULIANI G, SILVA LJHD & COUTO P. 1990. Origin of emerald deposits of Brazil. Miner Deposita 25(1): 57-64.

GROAT LA, GIULIANI G, MARSHALL DD & TURNER D. 2008. Emerald deposits and occurrences: A review. Ore Geol Rev 34: 87-112.

HAWTHORNE FC, OBERTI R, HARLOW GE, MARESCH WV, MARTIN RF, SCHUMACHER JC & WELCH MD. 2012. Nomenclature of the amphibole supergroup. Am Mineral 97: 2031-2048.

HUNT GR. 1977. Spectral signatures of particulate minerals, in the visible and near-infrared. Geophys 42: 501-513.

KERR A, RAFUSE H, SPARKES G, HINCHEY J & SANDEMAN H. 2011. Visible/infrared spectroscopy (VIRS) as a research tool in economic geology: background and pilot studies from Newfoundland and Labrador. Current Research, Newfoundland and Labrador Department of Natural Resources, Geological Survey. Report 11(1): 145-166.

MALVERN PANALYTICAL. 2020. ASD FieldSpec 4 Standard-Res Spectroradiometer. Malvern Panalytical. Available at: <https://www.asdi.com/productsand-services/fieldspec-spectroradiometers/fieldspec-4-standard-res/>. Accessed on: jan. 15, 2020.

MEDEIROS VC. 2008. Geologia e Recursos Minerais da Folha Sousa SB.24-Z-A. Escala 1:250.000. Recife: CPRM – Serviço Geológico do Brasil, 312 p.

MONIER G & ROBERT J. 1986. Evolution of the miscibility gap between muscovite and biotite solid solutions with increasing lithium content: an experimental study in the system K2O-Li2O-MgO-FeO-Al2O3-SiO2-H2O-HF at 600 ~ 2 kbar *PH2O*: comparison with natural lithium micas. Mineral Mag 50: 641-651.

MORAES JFS. 1999. Gemas do Estado do Rio Grande do Norte. Recife: CPRM – Serviço Geológico do Brasil, 72 p.

PONTUAL S, MERRY N & GAMSON P. 2008. Spectral interpretation – Field manual. GMEX. Spectral Analysis guides for mineral exploration. Victoria, AusSpec International Pty, 189 p.

RAMAKRISHNAN D & BHARTI R. 2015. Hyperspectral remote sensing and geological applications. Curr Sci 108(5): 879-891.

SANTIAGO JS, SOUZA VS, FILGUEIRAS BC & JIMENEZ FAC. 2018. Emerald from the Fazenda Bonfim Deposit, northeastern Brazil: chemical, fluid inclusions and oxygen isotope data. Braz J Geol 48(3): 457-472.

SANTOS EJ, SOUZA NETO JA, SILVA MRR, BEURLEN H, CAVALCANTI JAD, SILVA MG, DIAS VM, COSTA AF, SANTOS LCML & SANTOS RB. 2014. Metalogênese das porções norte e central da Província Borborema. In: Silva MG, Rocha Neto MB, Jost H and Kuyumijan RM (Eds), Metalogênese das províncias tectônicas brasileiras. Belo Horizonte: CPRM, p. 343-388.

SANTOS EJ, VAN SCHMUS WR, KOZUCH M & BRITO NEVES BB. 2010. The Cariris Velhos tectonic event in Northeast Brazil. J S Am Earth Sci 29(1): 61-76.

SCHWARZ D. 1987. Esmeraldas: inclusões em gemas. Ouro Preto: Universidade Federal de Ouro Preto (UFOP), Imprensa Universitária, 439 p.

SCORZA EP. 1944. Província Pegmatítica da Borborema (Nordeste do Brasil). Boletim 112. Rio de Janeiro, DNPM/DGM, 55 p.

SCOTT KM & YANG K. 1997. Spectral reflectance studies of white micas. Commonwealth Scientific and Industrial Research Organisation, Exploration and Mining Report 439R, 35 p.

SILVA MRR, HOLL R & BEURLEN H. 1995. Borborema Pegmatitic Province: geological and geochemical characteristics. J S Am Earth Sci 8(3-4): 355-364.

SILVA SMP, CRÓSTA AP, ANGÉLICA RS, BEURLEN H & SILVA MRR. 2009. Mineralogical characterization and mapping using reflectance spectroscopy: an experiment at Alto do Giz

Pegmatite in the south portion of Borborema Pegmatite Province (BPP), northeastern Brazil. Est Geol 19(2): 337-342.

SINKANKAS J. 1981. Emerald and other beryls. Radnor Pennsylvania. Chilton Book Company, p. 542-548.

SOUZA LC. 2017. Geologia e Recursos Minerais da Folha Pau dos Ferros SB.24-Z-A-II. Escala 1:100.000. Recife: CPRM - Serviço Geológico do Brasil / Universidade Federal do Rio Grande do Norte, 109 p.

SWAYZE GA ET AL. 2014. Mapping advanced argillic alteration at Cuprite, Nevada, using imaging spectroscopy. Econ Geol 109: 1179-1221.

THOMPSON AJB, HAUFF PL & ROBITAILLE AJ. 1999. Alteration mapping in exploration: application of short-wave infrared (SWIR) spectroscopy. Society of Economic Geologist Newsletter 39: 15-17.

TISCHENDORF G, FORSTER HJ & GOTTESMANN B. 1999. The correlation between lithium and magnesium in trioctrahedral micas: improved equations for Li2O estimation from MgO data. Mineral Mag 63: 57-74.

TISCHENDORF G, FORSTER HJ & GOTTESMANN B. 2001. Minor- and trace-element composition of trioctaehedral micas: a review. Mineral Mag 65(2): 249-276.

TURNER D, GROAT LA, RIVARD B & BELLEY PM. 2017. Reflectance spectroscopy and hyperspectral imaging of sapphire bearing marble from the Beluga occurrence, Baffin Island, Nunavut. Can Mineral 55: 787-797.

VAN SCHMUS WR, OLIVEIRA EP, SILVA FILHO AF, TOTEU F, PENAYE J & GUIMARAES IP. 2008. Proterozoic links between the Borborema Province, NE Brazil, and the Central African Fold Belt. Geol Soc London Spec Publ 294: 66-69.

VASCONCELOS FJC. 1984. Ocorrência de esmeralda em Pitombeiras, município de Paraná, Estado do Rio Grande do Norte. Especialização em Gemologia, Instituto de Geociências, Universidade Federal de Minas Gerais, Belo Horizonte, 36 p.

VIDAL FWH & NOGUEIRA NETO JA. 2005. Minerais de Pegmatitos. In: Vidal FWH (Org). Rochas e minerais industriais do Estado do Ceará. Fortaleza: CETEM/UECE/ DNPM/ FUNCAP/SENAI, p. 67-82.

WALTON L. 2004. Exploration criteria for coloured gemstone deposits in the Yukon. Yukon: Yukon Geological Survey, 184 p.

WOOD DL & NASSAU K. 1968. The characterization of beryl and emerald by visible and infrared absorption spectroscopy. Am Mineral 53(5-6): 777-800.

ZWAAN JC, JACOB DE, HAEGER T, CAVALCANTI NETO MTO & KANIS J. 2012. Emeralds from the Fazenda Bonfim Region, Rio Grande do Norte, Brazil. Gems Gemol 48(1): 2-17.

How to cite

ARAÚJO NETO JF, BARRETO SB, CARRINO TA, SOUZA IMBA & SANTOS GL. 2021. Geochemical and reflectance spectroscopy data integration to characterize emerald deposits: the case of the Paraná deposit, Brazil. An Acad Bras Cienc 93: 20200236. DOI 10.1590/0001-3765202120200236.

Manuscript received on February 17, 2020;
accepted for publication on October 15, 2020

JOSÉ F. ARAÚJO NETO[1,2]
https://orcid.org/0000-0002-1780-9469

SANDRA B. BARRETO[1,2]
https://orcid.org/0000-0001-8464-7087

THAIS A. CARRINO[1,2]
https://orcid.org/0000-0001-8528-5225

IGOR M.B.A. SOUZA[1,2]
https://orcid.org/0000-0002-2235-5668

GLENDA L. SANTOS[1,2]
https://orcid.org/0000-0002-6271-950X

[1]Programa de Pós-Graduação em Geociências, Universidade Federal de Pernambuco, Av. da Arquitetura, s/n, Cidade Universitária, 50740-550 Recife, PE, Brazil

[2]Universidade Federal de Pernambuco, Centro de Tecnologia e Geociências, Departamento de Geologia, Av. da Arquitetura, s/n, Cidade Universitária, 50740-550 Recife, PE, Brazil

Correspondence to: **José Ferreira de Araújo Neto**
E-mail: araujoneto.geo@gmail.com

Author contributions

JFAN wrote the first draft of the manuscript, worked on sample preparation, analysis and interpretations, prepared figures 1-12 and tables I-IV; SBB worked during field trips, sample collecting, provided support and advisement regarding whole-rock and mineral chemistry as also major interpretations; TAC performed reflectance spectroscopy in rock samples, prepared figure 13 and contributed to the spectral interpretation and text reviewing; IMBAS helped with field geology, petrographic descriptions and text reviewing; GLS worked during field trips and contributed to text reviewing.